ARCHIVES OF MECHANICS
Arch. Mech. **76** (3), 225–252, 2024, DOI: 10.24423/aom.4485

Nonlinear free vibration of functionally graded graphene nanoplatelet-reinforced composite rectangular plates using the full layerwise finite element method

M. S. TAYEBI[1)], S. JEDARI SALAMI[2)], M. TAVAKOLIAN[1)]

[1)] *Department of Mechanical Engineering, West Tehran Branch, Islamic Azad University, Tehran, Iran*

[2)] *Department of Mechanical Engineering, Central Tehran Branch, Islamic Azad University, Tehran, Iran, e-mail: sattar.salami@aut.ac.ir (corresponding author)*

This investigation is the first effort to study the nonlinear free vibration response of functionally graded (FG) graphene nanoplatelet (GPL)-reinforced composite rectangular plates using the full layerwise (LW) finite element method. The innovation of this article, which has not been investigated thus far, is a nonlinear vibration analysis with equivalent precision to three-dimensional (3D) elasticity while benefiting from decreased computational cost, ease of mesh adjustment, and faster achievement of the element stiffness matrix due to preserving the 2D structure. The modified Halpin–Tsai model and the rule of mixtures are employed to specify the effective material properties for composite plates with three different arrangements of GPLs. After confirming the results and formulation, an exhaustive parametric study is executed to examine how various characteristics of GPLs and the plate affect the nonlinear-to-linear frequency (NTL) ratio of the FG GPL-reinforced composite plate. The noteworthy finding is that inserting a small percentage of GPLs in pure epoxy changes its NTL ratio significantly. The effect of the GPL dimension on the NTL ratio is insignificant when the thickness-to-length ratio of GPLs is smaller than 10^{-3}.

Key words: nonlinear free vibration, full layerwise theory, functionally graded composite plate, finite element method, graphene nanoplatelets, GPL's gradient pattern.

1. Introduction:

Graphene nanoplatelets (GPLs) have attracted substantial consideration as reinforcement in the recent decade by giving nanocomposites extraordinary mechanical, thermal, and electrical characteristics at low density. Some researchers experimentally investigated the mechanical performance of GPL-embedded composites and found that mechanical properties of the structure (e.g., the modulus of elasticity, fracture toughness, tensile strength, and flexural strength) are significantly improved by incorporating GPLs into the matrix [1–5]. Consequently,

GPL-reinforced structures have been extensively employed in various fields involving automotive, aerospace, electronics, biomedical, and civil engineering.

The concept of functionally graded (FG) materials was introduced to carbon-based nanocomposite structures in 2009 [6]. It was found that a nonuniform gradient of carbon nanotubes (CNTs) can result in a further enhancement of the mechanical characteristics of the plate. Afterward, considerable investigations focused on the vibration conducts of FG CNT-reinforced composites [7–12]. The comparison between composite structures filled with GPL and CNT has shown that using GPLs as reinforcement leads to lower fabrication costs, superior dispersion of fillers in the polymer matrix, extremely better mechanical properties, and stronger adhesion between the polymer matrix and nanofillers [13, 14]. Thus, the study on the vibration conducts of FG GPL-reinforced nanocomposite structures has recently turned out to be an attractive research field. For instance, Song *et al.* [15] studied the vibration characteristics of FG GPL-reinforced composite plates according to the first-order shear deformation theory (FSDT) and the Navier solution. Similarly, Muni Rami Reddy *et al.* [16] employed the FSDT based on the finite element method (FEM) to explore the vibration conducts of FG GPL-reinforced thin and thick rectangular plates with various boundary condition (BC) combinations. Thai *et al.* [17] also discussed the free vibration conducts of FG GPL-reinforced composite plates using a nonuniform rational B-spline formulation predicated on the four-variable refined plate theory.

The above-mentioned works principally concentrated on the linear vibrations of FG GPL-reinforced composite structures. In actual engineering and industrial applications, these structures may be exposed to large deformations; therefore, investigating their nonlinear vibration conduct is necessary. Feng *et al.* [18] presented the nonlinear free vibration analysis of FG GPL-reinforced Timoshenko beams by means of the Ritz method. Gholami and Ansari [19–21] evaluated the nonlinear harmonically excited, forced, and free vibration characteristics of FG GPL-reinforced composite plates using the third-order shear deformation theory (TSDT). Likewise, Abdollahzadeh Jamalabadi *et al.* [22] obtained nonlinear free vibration responses of FG panels reinforced by GPLs using FSDT. Farsadi *et al.* [23] studied nonlinear natural frequencies of curved cylindrical panels made of FG GPL-reinforced polymer composites. Teng and Wang [24] investigated the nonlinear forced vibration of thin FG GPL-reinforced porous rectangular plates.

The above-reviewed literature indicates that most prior works investigating the nonlinear vibration characteristics of the FG GPL-reinforced composites are limited to equivalent single-layer (ESL) theories. These theories simplify the three-dimensional (3D) problem by reducing it to a 2D one, thus replacing the multilayer plate with an equivalent single layer. They assume the displacement field to be a C^1-continuous function through the thickness, lead-

ing to the ignorance of strain discontinuities and thus discontinuity of transverse stresses at the interface of dissimilar material layers (IDMLs). The error caused by the discontinuity of these stresses can be insignificant while analyzing the general behavior of plates (specifically thin plates). Nonetheless, ESL theories can produce incorrect results for all stresses for thick and composite plates (specifically at the ply level). To deal with this deficiency, Reddy [25] presented the layerwise (LW) theory in which the displacement field is assumed to be a C^0-continuous function through the thickness. Therefore, the continuity of transverse strains is not required, enabling the transverse stresses to be continuous at the IDMLs. However, few investigations have been directed toward the LW theory [26–30].

The principal novelty of the present article is to determine the 3D stress field through the thickness of the FG GPL-reinforced nanocomposite plate by employing the full LW theory and to accurately obtain its nonlinear free vibration response accordingly. In addition, using the FEM facilitates providing nonlinear vibration responses for various BC combinations of the plate. GPLs are assumed to be distributed according to three patterns over the thickness. The effective material properties of the plate are computed by applying the modified Halpin–Tsai model and the rule of mixtures. The governing equations of motion are derived considering the von Karman large deflection assumption and employing Hamilton's principle. Finally, the influence of some significant factors, including the gradient pattern, concentration, and geometry of GPLs, as well as the plate's thickness and BCs, on the nonlinear free vibration response of FG GPL-reinforced rectangular composite plates, is discussed through a thorough numerical study.

2. Theoretical formulatio

An FG GPL-reinforced nanocomposite plate is illustrated in Fig. 1, in which a, b, and h are the plate's length, width, and thickness, respectively. The plate is composed of N_L plies with identical thicknesses of $\Delta h = h/N_L$.

Each ply is presumed to be isotropic homogeneous owing to the uniform dispersion of GPLs in the polymer matrix. Simultaneously, the GPL' weight fraction changes from ply to ply over the thickness direction based on one of the three specified patterns (Fig. 2), where the darker shade indicates a greater concentration of GPLs. The uniformly distributed (UD) pattern is a specific case where the weight fraction of GPLs is equal in all plate plies, forming an isotropic homogeneous plate. Their weight fraction rises and reduces from the upper and lower plies to the central plies for the symmetrical FG-O and FG-X patterns, respectively. Consequently the central plies of FG-O and the upper and lower plies of FG-X have the highest GPLs concentration.

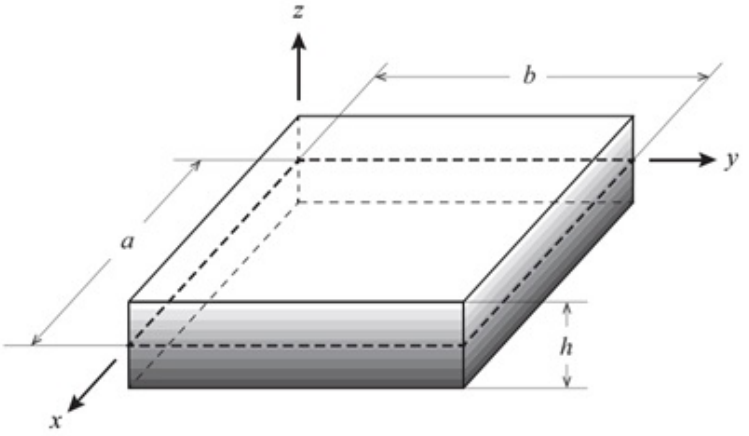

Fig. 1. Schematic of the FG GPL-reinforced nanocomposite rectangular plate.

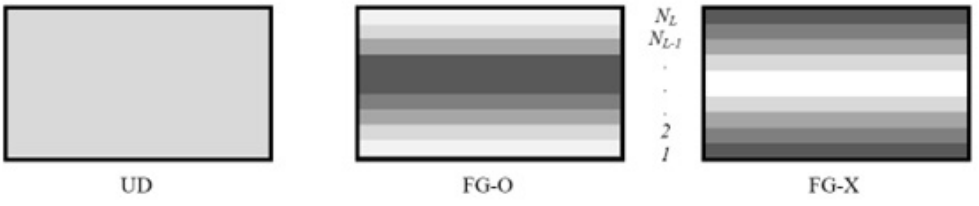

Fig. 2. Three nanocomposite plates with various GPL gradient patterns.

Signifying the volume fraction of GPLs distributed in the whole plate by V_{GPL}, the volume fraction of GPLs in the l-th ply under the three GPL gradient patterns can be computed as follows [31]:

UD pattern:

$$V_{\mathrm{GPL}}^{(l)} = V_{\mathrm{GPL}}, \tag{2.1}$$

FG-O pattern:

$$V_{\mathrm{GPL}}^{(l)} = 2V_{\mathrm{GPL}}(1 - |2l - N_L - 1|/N_L), \tag{2.2}$$

FG-X pattern:

$$V_{\mathrm{GPL}}^{(l)} = 2V_{\mathrm{GPL}}|2l - N_L - 1|/N_L, \tag{2.3}$$

where $l = 1, 2, \ldots, N_L$, and V_{GPL} is expressed by [31],

$$V_{\mathrm{GPL}} = \frac{W_{\mathrm{GPL}}}{W_{\mathrm{GPL}} + (\rho_{\mathrm{GPL}}/\rho_M)(1 - W_{\mathrm{GPL}})}, \tag{2.4}$$

where W_{GPL} is the total weight fraction of GPLs distributed in the plate. Furthermore, ρ_{GPL} and ρ_M are the GPL and epoxy matrix mass densities, respectively.

This research develops the LW FEM for the nonlinear vibration examination of FG GPL-reinforced rectangular nanocomposite plates. Regarding the results' accuracy, this method is equivalent to the 3D FEM, offering the advantage of a smaller input data volume and less computation time owing to a lower degree of freedom. The LW finite element model is constructed by combining a 1D finite element (through the thickness) with a 2D finite element (in-plane). In this regard, the initial step includes assembling one element through the thickness to create an LW element. The next step is assembling LW elements within the $(x-y)$-plane, enabling the calculation of the total stiffness matrix.

2.1. Material properties

The effective Young modulus of the l-th ply is approximated by the modified Halpin–Tsai model as [32–35]

$$E_C^{(l)} = \left[\frac{3}{8}\left(\frac{1+\xi_L\eta_L V_{\mathrm{GPL}}^{(l)}}{1-\eta_L V_{\mathrm{GPL}}^{(l)}}\right) + \frac{5}{8}\left(\frac{1+\xi_W\eta_W V_{\mathrm{GPL}}^{(l)}}{1-\eta_W V_{\mathrm{GPL}}^{(l)}}\right)\right] E_M, \tag{2.5}$$

where the GPLs' geometric parameters (ξ_L and ξ_W) are defined as:

$$\xi_L = 2/\left(\frac{h_{\mathrm{GPL}}}{a_{\mathrm{GPL}}}\right), \tag{2.6}$$

$$\xi_W = 2/\left(\frac{h_{\mathrm{GPL}}}{b_{\mathrm{GPL}}}\right) \tag{2.7}$$

and

$$\eta_L = \frac{(E_{\mathrm{GPL}}/E_M)-1}{(E_{\mathrm{GPL}}/E_M)+\xi_L}, \tag{2.8}$$

$$\eta_W = \frac{(E_{\mathrm{GPL}}/E_M)-1}{(E_{\mathrm{GPL}}/E_M)+\xi_W}. \tag{2.9}$$

E_M and E_{GPL} indicate Young's modulus of epoxy and GPLs, respectively. Moreover, h_{GPL}, a_{GPL}, and b_{GPL} refer to the average thickness, length, and width of GPLs, respectively.

According to the rule of mixtures, the effective Poisson ratio ν_C and mass density ρ_C of the l-th ply can be estimated as [36]:

$$\nu_C^{(l)}) = \nu_{\mathrm{GPL}} V_{\mathrm{GPL}}^{(l)} + \nu_M(1 - V_{\mathrm{GPL}}^{(l)}), \tag{2.10}$$

$$\rho_C^{(l)} = \rho_{\mathrm{GPL}} V_{\mathrm{GPL}}^{(l)} + \rho_M(1 - V_{\mathrm{GPL}}^{(l)}), \tag{2.11}$$

where ν_{GPL} and ν_M denote Poisson's ratios of GPL and epoxy, respectively.

2.2. Governing equation

The rectangular plate is assumed to be divided into N layers of equal depth to apply the LW theory (Fig. 3).

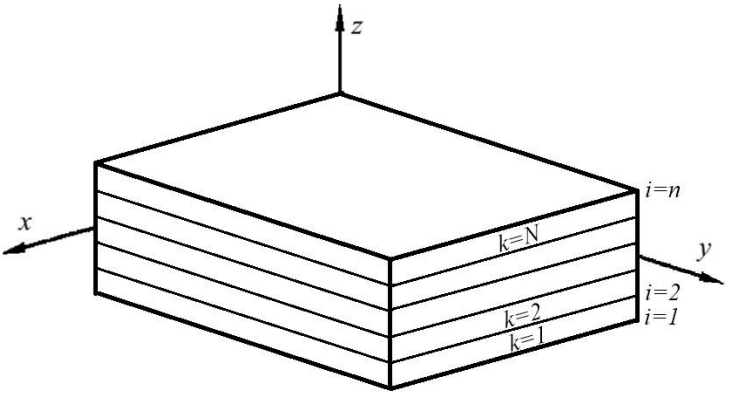

Fig. 3. A rectangular plate divided into N equal depth layers; n is the number of planes produced by the division of the plate ($n = N + 1$).

The displacement components of all points placed on the i-th plane in the x, y, and z direction are signified by U^i, V^i, and W^i, respectively; according to the LW theory, the displacement components of the plateat time t in the x, y, and z directions are described as follows [37]:

$$
\begin{aligned}
u(x,y,z,t) &= \sum_{i=1}^{n} U^i(x,y,t)\phi^i(z),\\
v(x,y,z,t) &= \sum_{i=1}^{n} V^i(x,y,t)\phi^i(z),\\
w(x,y,z,t) &= \sum_{i=1}^{n} W^i(x,y,t)\phi^i(z),
\end{aligned}
\tag{2.12}
$$

where $\phi^i(z)$ is a linear Lagrangian interpolation function that exerts 1D finite element through the thickness, defined as [26]:

$$
\phi^i(z) = \begin{cases}
0 & z \le z_{i-1},\\
\psi_1^i = \dfrac{(z - z_{i-1})}{(z_i - z_{i-1})} & z_{i-1} \le z \le z_i,\\
\psi_2^i = \dfrac{(z_{i+1} - z)}{(z_{i+1} - z_i)} & z_i \le z \le z_{i+1},\\
0 & z \ge z_{i+1}.
\end{cases}
\tag{2.13}
$$

Substituting Eq. (2.12) into von Karman nonlinear strain-displacement relations [37] results in:

$$
\begin{aligned}
\varepsilon_{xx} &= \sum_{i=1}^{n} \frac{\partial U^i}{\partial x}\phi^i + \frac{1}{2}\left(\sum_{i=1}^{n} \frac{\partial W^i}{\partial x}\phi^i\right)\left(\sum_{j=1}^{n} \frac{\partial W^j}{\partial x}\phi^j\right),\\
\varepsilon_{yy} &= \sum_{i=1}^{n} \frac{\partial V^i}{\partial y}\phi^i + \frac{1}{2}\left(\sum_{i=1}^{n} \frac{\partial W^i}{\partial y}\phi^i\right)\left(\sum_{j=1}^{n} \frac{\partial W^j}{\partial y}\phi^j\right),\\
\varepsilon_{zz} &= \sum_{i=1}^{n} W^i \frac{d\phi^i}{dz},\\
\gamma_{yz} &= \sum_{i=1}^{n} \frac{\partial W^i}{\partial y}\phi^i + \sum_{i=1}^{n} V^i \frac{d\phi^i}{dz},\\
\gamma_{xz} &= \sum_{i=1}^{n} \frac{\partial W^i}{\partial x}\phi^i + \sum_{i=1}^{n} U^i \frac{d\phi^i}{\partial z},\\
\gamma_{xy} &= \sum_{i=1}^{n} \frac{\partial U^i}{\partial y}\phi^i + \sum_{i=1}^{n} \frac{\partial V^i}{\partial x}\phi^i + \left(\sum_{i=1}^{n} \frac{\partial W^i}{\partial x}\phi^i\right)\left(\sum_{j=1}^{n} \frac{\partial W^j}{\partial y}\phi^j\right).
\end{aligned}
\tag{2.14}
$$

The 3D constitutive relations are employed to obtain the stresses in the k-th layer as [38]:

$$
\begin{Bmatrix} \sigma_{xx} \\ \sigma_{yy} \\ \sigma_{zz} \\ \sigma_{yz} \\ \sigma_{xz} \\ \sigma_{xy} \end{Bmatrix}^{(k)} = \begin{bmatrix} Q_{11} & Q_{12} & Q_{13} & 0 & 0 & 0 \\ Q_{12} & Q_{22} & Q_{23} & 0 & 0 & 0 \\ Q_{13} & Q_{23} & Q_{33} & 0 & 0 & 0 \\ 0 & 0 & 0 & Q_{44} & 0 & 0 \\ 0 & 0 & 0 & 0 & Q_{55} & 0 \\ 0 & 0 & 0 & 0 & 0 & Q_{66} \end{bmatrix}^{(k)} \begin{Bmatrix} \varepsilon_{xx} \\ \varepsilon_{yy} \\ \varepsilon_{zz} \\ \gamma_{yz} \\ \gamma_{xz} \\ \gamma_{xy} \end{Bmatrix}^{(k)},
\tag{2.15}
$$

where $Q_{\alpha\beta}^{(k)}$ are the material stiffnesses of the k-th layer, calculated as:

$$
\begin{aligned}
Q_{11}^{(k)} = Q_{22}^{(k)} = Q_{33}^{(k)} &= \frac{E_C^{(k)}}{1-\nu_C^2},\\
Q_{12}^{(k)} = Q_{13}^{(k)} = Q_{23}^{(k)} &= \frac{\nu_C E_C^{(k)}}{1-\nu_C^2},\\
Q_{44}^{(k)} = Q_{55}^{(k)} = Q_{66}^{(k)} &= \frac{E_C^{(k)}}{2(1+\nu_C)}.
\end{aligned}
\tag{2.16}
$$

2.3. Equation of motion

The dynamic equations of the plate affected by the free vibration regime can be acquired from the following statement of Hamilton's principle [37]:

$$\int_0^T (\delta U_{\text{total}} - \delta T_{\text{total}})\, dt = 0, \tag{2.17}$$

where U_{total} and T_{total} refer to total strain and kinetic energy, respectively, and δ is the variational symbol that turns them into virtual parameters.

The strain energy for an LW element is considered as [37]:

$$\begin{aligned} U &= \frac{1}{2}\int_A \left[\int_{-h/2}^{h/2} (\sigma_{xx}\varepsilon_{xx}\sigma_{yy}\varepsilon_{yy}+\sigma_{zz}\varepsilon_{zz}+\tau_{yz}\gamma_{yz}+\tau_{xz}\gamma_{xz}+\tau_{xy}\gamma_{xy})\, dz\right] dx\, dy \\ &= \frac{1}{2}\int_A \left\{\sum_{i=1}^{n}\left[N_{xx}^i\frac{\partial U^i}{\partial x}+N_{yy}^i\frac{\partial V^i}{\partial y}+N_{xy}^i\left(\frac{\partial U^i}{\partial y}+\frac{\partial V^i}{\partial x}\right)\right.\right. \\ &\quad \left. + \bar{Q}_x^i\frac{\partial W^i}{\partial x}+\bar{Q}_y^i\frac{\partial W^i}{\partial y}+Q_x^iU^i+Q_y^iV^i+Q_z^iW^i\right] \\ &\quad \left. + \frac{1}{2}\sum_{i,j=1}^{n}\left(\bar{N}_{xx}^{ij}\frac{\partial W^j}{\partial x}\frac{\partial W^i}{\partial x}+\bar{N}_{yy}^{ij}\frac{\partial W^j}{\partial y}\frac{\partial W^i}{\partial y}+2\bar{N}_{xy}^{ij}\frac{\partial W^j}{\partial x}\frac{\partial W^i}{\partial y}\right)\right\} dx\, dy, \end{aligned} \tag{2.18}$$

where N, $\bar{N}$, Q, and $\bar{Q}$ refer to stress resultants, described as:

$$\begin{aligned} N_{xx}^i, N_{yy}^i, N_{xy}^i &= \int_{-h/2}^{h/2} (\sigma_{xx}, \sigma_{yy}, \tau_{xy})\phi^i\, dz, \\ \bar{N}_{xx}^{ij}, \bar{N}_{yy}^{ij}, \bar{N}_{xy}^{ij} &= \int_{-h/2}^{h/2} (\sigma_{xx}, \sigma_{yy}, \tau_{xy})\phi^i\phi^j\, dz, \\ Q_x^i, Q_y^i, Q_z^i &= \int_{-h/2}^{h/2} (\tau_{xz}, \tau_{yz}, \sigma_{zz})\frac{d\phi^i}{dz}\, dz, \\ \bar{Q}_x^i, \bar{Q}_y^i &= \int_{-h/2^h/2} (\tau_{xz}, \tau_{yz})\phi^i\, dz. \end{aligned} \tag{2.19}$$

By substituting Eq. (2.14) into Eq. (2.15) and the subsequent results in Eq. (2.18), it can be rewritten as:

$$U = \frac{1}{2}\int_A ([K_1]+[K_2]+[K_3]+[K_3]^T+[K_4]+[K_1^{NL}]+[K_2^{NL}]+[K_3^{NL}])\, dx\, dy, \tag{2.20}$$

where $[K]$ and $[K^{NL}]$ denote linear and nonlinear stiffness sub-matrices, respectively, defined as:

(2.21)

$$[K_1] = \sum_{i=1}^{n}\sum_{j=1}^{n}\left(\begin{Bmatrix} \frac{\partial U^i}{\partial x} \\ \frac{\partial V^i}{\partial y} \\ W^i \\ \frac{\partial U^i}{\partial y}+\frac{\partial V^i}{\partial x} \end{Bmatrix}^T \begin{bmatrix} A_{11}^{ij} & A_{12}^{ij} & \hat{A}_{13}^{ij} & 0 \\ A_{12}^{ij} & A_{22}^{ij} & \hat{A}_{23}^{ij} & 0 \\ \hat{A}_{13}^{ji} & \hat{A}_{23}^{ji} & \bar{A}_{33}^{ij} & 0 \\ 0 & 0 & 0 & A_{66}^{ij} \end{bmatrix} \begin{Bmatrix} \frac{\partial U^j}{\partial x} \\ \frac{\partial V^j}{\partial y} \\ W^j \\ \frac{\partial U^j}{\partial y}+\frac{\partial V^j}{\partial x} \end{Bmatrix}\right),$$

$$[K_2] = \sum_{i=1}^{n}\sum_{j=1}^{n}\left(\begin{Bmatrix} U^i \\ V^i \end{Bmatrix}^T \begin{bmatrix} \bar{A}_{55}^{ij} & 0 \\ 0 & \bar{A}_{44}^{ij} \end{bmatrix} \begin{Bmatrix} U^j \\ V^j \end{Bmatrix}\right),$$

$$[K_3] = \sum_{i=1}^{n}\sum_{j=1}^{n}\left(\begin{Bmatrix} U^i \\ V^i \end{Bmatrix}^T \begin{bmatrix} \bar{B}_{55}^{ij} & 0 \\ 0 & \bar{B}_{44}^{ij} \end{bmatrix} \begin{Bmatrix} \frac{\partial W^j}{\partial x} \\ \frac{\partial W^j}{\partial y} \end{Bmatrix}\right),$$

$$[K_4] = \sum_{i=1}^{n}\sum_{j=1}^{n}\left(\begin{Bmatrix} \frac{\partial W^i}{\partial x} \\ \frac{\partial W^i}{\partial y} \end{Bmatrix}^T \begin{bmatrix} D_{55}^{ij} & 0 \\ 0 & D_{44}^{ij} \end{bmatrix} \begin{Bmatrix} \frac{\partial W^j}{\partial x} \\ \frac{\partial W^j}{\partial y} \end{Bmatrix}\right),$$

$$[K_1^{NL}] = \sum_{i=1}^{n}\sum_{j=1}^{n}\sum_{p=1}^{n}\begin{Bmatrix} \frac{\partial U^i}{\partial x} \\ \frac{\partial V^i}{\partial y} \\ \frac{\partial U^i}{\partial y}+\frac{\partial V^i}{\partial x} \end{Bmatrix}^T \begin{bmatrix} B_{11}^{ijp} & B_{12}^{ijp} & 0 \\ B_{12}^{ijp} & B_{22}^{ijp} & 0 \\ 0 & 0 & B_{66}^{ijp} \end{bmatrix} \begin{Bmatrix} \frac{1}{2}\frac{\partial W^j}{\partial x}\frac{\partial W^p}{\partial x} \\ \frac{1}{2}\frac{\partial W^j}{\partial x}\frac{\partial W^p}{\partial x} \\ \frac{\partial W^j}{\partial x}\frac{\partial W^p}{\partial y} \end{Bmatrix},$$

$$[K_2^{NL}] = \sum_{i=1}^{n}\sum_{j=1}^{n}\sum_{p=1}^{n}\begin{Bmatrix} \frac{1}{2}\frac{\partial W^i}{\partial x}\frac{\partial W^j}{\partial x} \\ \frac{1}{2}\frac{\partial W^i}{\partial y}\frac{\partial W^j}{\partial y} \\ \frac{\partial W^i}{\partial x}\frac{\partial W^j}{\partial y} \end{Bmatrix}^T \begin{bmatrix} B_{11}^{pij} & B_{12}^{pij} & \hat{B}_{13}^{pij} & 0 \\ B_{12}^{pij} & B_{22}^{pij} & \hat{B}_{23}^{pij} & 0 \\ 0 & 0 & 0 & B_{66}^{pij} \end{bmatrix} \begin{Bmatrix} \frac{\partial U^p}{\partial x} \\ \frac{\partial V^p}{\partial y} \\ W^p \\ \frac{\partial U^p}{\partial y}+\frac{\partial V^p}{\partial x} \end{Bmatrix},$$

$$[K_3^{NL}] = \sum_{i=1}^{n}\sum_{j=1}^{n}\sum_{p=1}^{n}\sum_{q=1}^{n}\begin{Bmatrix} \frac{1}{2}\frac{\partial W^i}{\partial x}\frac{\partial W^j}{\partial x} \\ \frac{1}{2}\frac{\partial W^i}{\partial y}\frac{\partial W^j}{\partial y} \\ \frac{\partial W^i}{\partial x}\frac{\partial W^j}{\partial y} \end{Bmatrix}^T \begin{bmatrix} D_{11}^{ijpq} & D_{12}^{ijpq} & 0 \\ D_{12}^{ijpq} & D_{22}^{ijpq} & 0 \\ 0 & 0 & D_{66}^{ijpq} \end{bmatrix} \begin{Bmatrix} \frac{1}{2}\frac{\partial W^p}{\partial x}\frac{\partial W^q}{\partial x} \\ \frac{1}{2}\frac{\partial W^p}{\partial y}\frac{\partial W^q}{\partial y} \\ \frac{\partial W^p}{\partial x}\frac{\partial W^q}{\partial y} \end{Bmatrix},$$

stiffnesses $A_{\alpha\beta}^{ij}$, $\hat{A}_{\alpha\beta}^{ij}$, $\bar{A}_{\alpha\beta}^{ij}$, $\bar{B}_{\alpha\beta}^{ij}$, $D_{\alpha\beta}^{ij}$, $B_{\alpha\beta}^{ijp}$, $\hat{B}_{\alpha\beta}^{ijp}$, and $D_{\alpha\beta}^{ijpq}$ for the k-th layer are defined as:

(2.22)
$$A_{\alpha\beta}^{ij}{}^{(k)} = \int_{z_b^k}^{z_t^k} Q_{\alpha\beta}^{(k)}\phi^i\phi^j\,dz,$$

$$\hat{A}^{ij}_{\alpha\beta}{}^{(k)} = \int_{z_b^k}^{z_t^k} Q^{(k)}_{\alpha\beta}\phi^i \frac{d\phi^j}{dz}\, dz,$$

$$\bar{A}^{ij}_{\alpha\beta}{}^{(k)} = \int_{z_b^k}^{z_t^k} Q^{(k)}_{\alpha\beta}\frac{d\phi^i}{dz}\,\frac{d\phi^j}{dz}\, dz,$$

$$\bar{B}^{ij}_{\alpha\beta}{}^{(k)} = \int_{z_b^k}^{z} {}^k_t Q^{(k)}_{\alpha\beta}\frac{d\phi^i}{dz}\phi^j\, dz,$$

(2.22)$_{[\text{cont.}]}$

$$D^{ij}_{\alpha\beta}{}^{(k)} = \int_{z_b^k}^{z_t^k} Q^{(k)}_{\alpha\beta}\phi^i\phi^j\, dz,$$

$$B^{ijp(k)}_{\alpha\beta} = \int_{z_b^k}^{z_t^k} Q^{(k)}_{\alpha\beta}\phi^i\phi^j\phi^p\, dz,$$

$$\hat{B}^{ijp(k)}_{\alpha\beta} = \int_{z_b^k}^{z_t^k} Q^{(k)}_{\alpha\beta}\phi^i\phi^j\frac{d\phi^p}{dz}\, dz,$$

$$D^{ijpq(k)}_{\alpha\beta} = \int_{z_b^k}^{z_t^k} Q^{(k)}_{\alpha\beta}\phi^i\phi^j\phi^p\phi^q\, dz,$$

where z_b^k and z_t^k indicate the height of the bottom and top surfaces of the k-th layer, respectively.

The kinetic energy for an LW element is expressed as [37]

$$T = \frac{1}{2}\int_A \left[\int_{-h/2}^{h/2} \rho(\dot{u}^2 + \dot{v}^2 + \dot{w}^2)\, dz\right] dx\, dy, \tag{2.23}$$

where the time derivatives of u, v, and$w$ are demonstrated by $\dot{u}$, $\dot{v}$, and $\dot{w}$, respectively, and ρ refers to mass density. The displacement components in Eq. (2.23) are replaced with those of Eq. (2.12), and the kinetic energy is converted into

$$T = \frac{1}{2}\int_A \sum_{i=1}^{n}\sum_{j=1}^{n}\left(\left\{\begin{array}{c} U^i \\ V^i \\ W^i \end{array}\right\}^T \left[I^{ij}\right]\left\{\begin{array}{c} \ddot{U}^j \\ \ddot{V}^j \\ \ddot{W}^j \end{array}\right\}\right) dx\, dy. \tag{2.24}$$

The inertia matrix $[I^{ij}]$ for the k-th layer is defined as

$$I^{ij^{(k)}} = \int_{z_b^k}^{z_t^k} \rho^{(k)} \phi^i \phi^j \, dz. \tag{2.25}$$

The integrals in Eqs. (2.22) and (2.25) are solved using the Gaussian numerical integration method, and the consequent matrices are assembled through the thickness [37], giving the strain and kinetic energy of an LW element as:

$$U = \frac{1}{2}\{d_{lw}\}^T([K_{lw}] + [K_{lw}^{NL}])\{d_{lw}\}, \tag{2.26}$$

$$T = \frac{1}{2}\{\dot{d}_{lw}\}^T[M_{lw}]\{\dot{d}_{lw}\}, \tag{2.27}$$

where $[K_{lw}^{NL}]$, $[K_{lw}]$, $[M_{lw}]$, $\{d_{lw}\}$, and $\{\dot{d}_{lw}\}$ refer to the nonlinear stiffness matrix, linear stiffness matrix, mass matrix, displacement vector, and time derivative of the displacement vector relevant to the LW element, respectively. These matrices and vectors are assembled within the $(x-y)$-plane [28], and the plate's total strain and kinetic energy are achieved as:

$$U_{\text{total}} = \frac{1}{2}\{d_{\text{total}}\}^T([K_{\text{total}}] + [K_{\text{total}}^{NL}])\{d_{\text{total}}\}, \tag{2.28}$$

$$T_{\text{total}} = \frac{1}{2}\{\dot{d}_{\text{total}}\}^T[M_{\text{total}}]\{\dot{d}_{\text{total}}\}. \tag{2.29}$$

By applying Hamilton's principle, the motion equation of all nodes of the plate is derived as

$$[M_{\text{total}}]\{\ddot{d}_{\text{total}}\} + ([K_{\text{total}}] + [K_{\text{total}}^{NL}])\{d_{\text{total}}\} = 0. \tag{2.30}$$

Based on the iterative displacement control approach [39], the continuum equivalent of Eq. (2.30) is lowered to a nonlinear eigenvalue problem by noticing that the maximum amplitude point is of particular attention and determining the specific characteristics of the time function at this point as

$$\{\ddot{d}_{\text{total}}^{\max}\} = -\omega^2\{d_{\text{total}}^{\max}\}. \tag{2.31}$$

Substituting Eq. (2.31) in Eq. (2.30) yields the following nonlinear eigenvalue problem

$$([K_{\text{total}} + K_{\text{total}}^{NL}] - \omega^2[M_{\text{total}}])\{d_{\text{total}}^{\max}\} = 0, \tag{2.32}$$

while the obtained equation can be resolved iteratively by considering the displacement vector $\{d_{\text{total}}^{\max}\}$, which is mentioned in the next section.

Firstly, a linear vibration analysis should be performed. In this regard, the total nonlinear stiffness matrix ($[K^{NL}_{\text{total}}]$) is presumed to be zero, and the presumption $\{\ddot{d}_{\text{total}}\} = -\omega^2\{d_{\text{total}}\}$ is applied; therefore, Eq. (2.30) transforms into a standard eigenvalue problem as follows:

$$([K_{\text{total}}] - \omega^2[M_{\text{total}}])\{\bar{d}\} = 0 \tag{2.33}$$

linear natural frequencies ω and the related mode shape vectors $\{\bar{d}\}$ are obtained after exerting BCs and solving the above-mentioned equation. The succeeding process should be performed to acquire the nonlinear free vibration response of the plate:

1) A component of the total displacement vector $\{d^{\max}_{\text{total}}\}$ is presumed to possess a specified value. In the present research, $w^1_{\max}$ is supposed to be recognized.
2) The eigenvector related to the linear analysis is normalized and scaled up concerning the presumed displacement of the previous step.
3) The total nonlinear stiffness matrix $[K^{NL}_{\text{total}}]$ is achieved considering the displacement vector of step 2.
4) A novel eigenvalue analysis is performed to update the natural frequency and eigenvector.
5) It is essential to note that the results acquired in the previous step are solely estimated owing to step (2). The eigenvector developed by step (4) is scaled up by the presumed displacement $w^1_{\max}$.
6) The process of steps (3)–(5) is iterated to achieve a convergent frequency parameter, known as the nonlinear frequency, and its associated eigenvector.

In the present research, the convergence parameter is presumed as

$$\frac{\omega^{i+1}_{nl} - \omega^i_{nl}}{\omega^{i+1}_{nl}} \leq 10^{-8}.$$

The iterative process can be ceased once this value is achieved.

3. Numerical results and discussion

3.1. Convergence and validation analysis

Firstly, the convergence of the LW FEM is examined, and then a comparative assessment is performed by comparing the vibration characteristics acquired in this investigation with those in previous works to validate the veracity of the

method. A square-shaped FG GPL-reinforced composite plate with a length of 0.45 m is contemplated in this regard. The average dimensions of GPLs are presumed as:

$$h_{\mathrm{GPL}} = 1.5\,\mathrm{nm}, \qquad a_{\mathrm{GPL}} = 2.5\,\mu\mathrm{m}, \qquad b_{\mathrm{GPL}} = 1.5\,\mu\mathrm{m}. \tag{3.1}$$

The material characteristics of the GPL and polymer matrix are as follows [1, 40, 41]:

$$\begin{aligned} \rho_{\mathrm{GPL}} &= 1060\,\mathrm{kg/m^3}, \quad E_{\mathrm{GPL}} = 1.01\,\mathrm{TPa}, \quad \nu_{\mathrm{GPL}} = 0.186, \\ \rho_M &= 1200\,\mathrm{kg/m^3}, \quad E_M = 3\,\mathrm{GPa}, \quad \nu_M = 0.34. \end{aligned} \tag{3.2}$$

The plates with three BC combinations have been investigated in this study. For example, CCSS represents a plate with clamped, clamped, simply supported, and simply supported constraints at left, right, upper, and lower edges, respectively.

The linear and nonlinear frequencies of the FG GPL-reinforced composite plate are signified by ω_L and ω_{NL}, respectively; the following dimensionless parameters are introduced for ease of comparison:

$$\begin{gathered} W_{\max} = \frac{w_{\max}}{h}, \\ \{\Omega_L, \Omega_{NL}\} = \{\omega_L, \omega_{NL}\} a \sqrt{\frac{\rho_M (1-\nu_M)}{E_M}}, \\ \bar{\Omega}_L = \omega_L h \sqrt{\frac{\rho_M}{E_M}}. \end{gathered} \tag{3.3}$$

Figures 4a-c depict the nonlinear-to-linear (NTL) ratio (Ω_{NL}/Ω_L) of thin, moderately thick, and thick SSSS GPL/Epoxy FG square plates, with variations in the mesh size and the number of layers (N_L) to evaluate the convergence of the current method. The gradient pattern of GPLs is FG-X. In addition, the dimensionless maximum amplitude ($W_{\max}$) is 0.6, and $W_{\mathrm{GPL}} = 0.3\%$.

Based on data in Fig. 4 convergent results are achieved when the mesh size is 10×10, and the number of layers rises to 20. Therefore, considering the volume of calculations and simplicity of production, the FG GPL-reinforced composite rectangular plates with a mesh size of 10×10 and 20 material layers are considered in the following numerical analysis.

The first four fundamental frequency parameters ($\bar{\Omega}_L$) of the SSSS FG GPL-reinforced composite plate are computed in this step (Table 1). Then, they are compared with TSDT-based [7, 21] and FSDT-based [15, 16] results to investigate the validation of the current method.

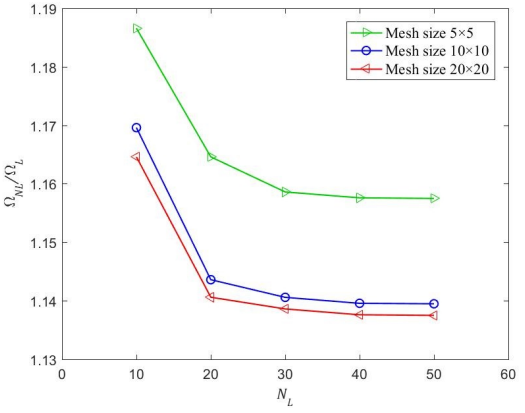

(a) $h/a = 0.05$

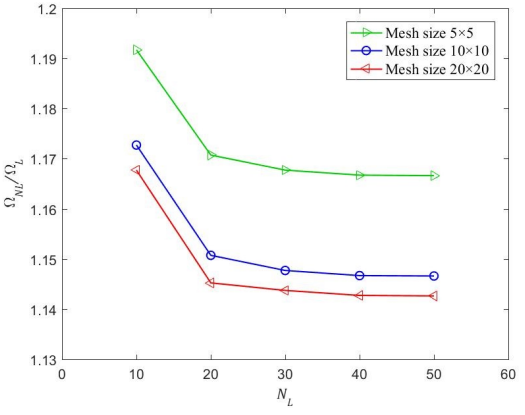

(b) $h/a = 0.1$

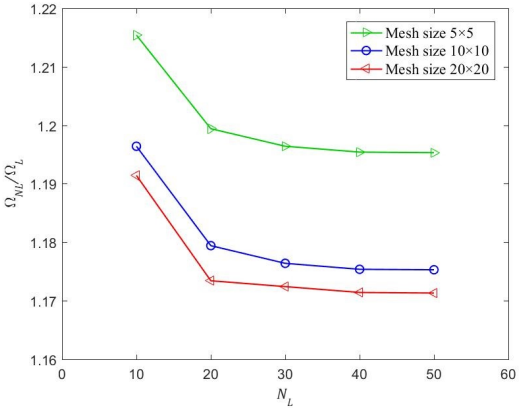

(c) $h/a = 0.2$

Fig. 4. The NTL ratio of GPL/Epoxy FG square plates against the number of layers while the GPL gradient pattern is FG-X ($W_{\max} = 0.6$, $W_{\mathrm{GPL}} = 0.3$).

TABLE 1. Fundamental frequency parameters $\bar{\Omega}_L$ of SSSS GPL/epoxy FG square plates with various GPL gradient patterns ($h/a = 0.1$, $W_{\mathrm{GPL}} = 1\%$).

Method	Mode	Pure epoxy	UD pattern	FG-O pattern	FG-X pattern
Present	1	0.0594	0.1236	0.0927	0.1457
[7]	(1, 1)	0.0588	0.1223	0.0908	0.1452
[21]	1	0.0580	0.1216	0.0978	0.1369
[15]	(1, 1)	0.0584	0.1216	0.1020	0.1378
[16]	1	0.0588	0.1225	0.0912	0.1420
Present	2	0.1426	0.2968	0.2297	0.3317
[7]	(2, 1)	0.1409	0.2932	0.2208	0.3410
[21]	2	0.1390	0.2894	0.2368	0.3232
[15]	(2, 1)	0.1391	0.2896	0.2456	0.3249
[16]	2	0.1412	0.2941	0.2246	0.3245
Present	3	0.2197	0.4572	0.3627	0.4936
[7]	(2, 2)	0.2171	0.4518	0.3443	0.5166
[21]	3	0.2131	0.4433	0.3680	0.4856
[15]	(2, 2)	0.2132	0.4436	0.3796	0.4939
[16]	3	0.2176	0.4531	0.3532	0.4810
Present	4	0.2684	0.5584	0.4492	0.5853
[7]	(3, 1)	0.2651	0.5519	0.4235	0.6250
[21]	4	0.2580	0.5397	0.4516	0.5848
[15]	(3, 1)	0.2595	0.5400	0.4645	0.5984
[16]	4	0.2658	0.5535	0.4378	0.5750

Based on data in Table 1, the relative difference between most of the present numerical results and those of previous works is less than 6.9%, proving the reliability of the current approach.

Figures 5a-c display the NTL ratio of GPL/Epoxy FG square plates against dimensionless maximum amplitude, while the gradient pattern of GPLs is FG-X, $W_{\mathrm{GPL}} = 0.3\%$, $h/a = 0.1$, and BCs are SSSS, CCSS, and CCCC, respectively. Furthermore, the present results are compared with the FSDT and TSDT-based results of GHOLAMI and ANSARI [21].

Based on the results, a good consistency is found between the present and ESL-based results. The NTL ratio exhibits a quasi-parabolic increase with dimensionless maximum amplitude. Compared to FSDT and TSDT, the current method provides a more realistic estimation of linear and nonlinear stiffness matrices, resulting in higher NTL ratios.

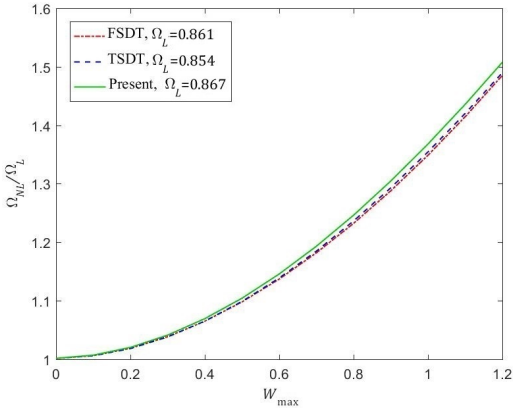

(a) SSSS

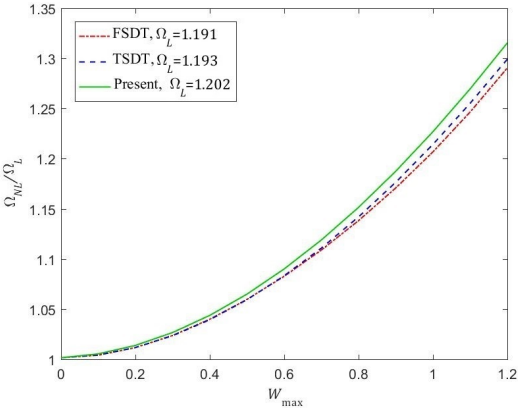

(b) CCSS

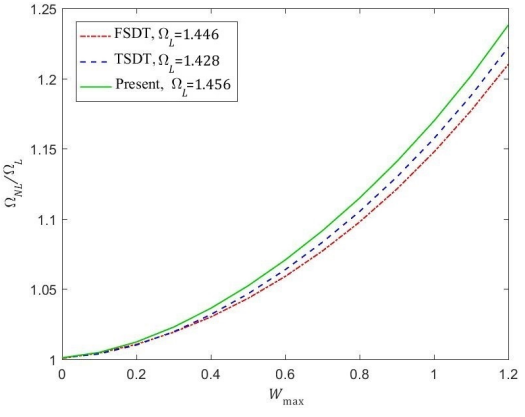

(c) CCCC

Fig. 5. The NTL ratio of GPL/Epoxy FG square plates against dimensionless maximum amplitude while the GPL gradient pattern is FG-X ($h/a = 0.1$, $W_{\mathrm{GPL}} = 0.3$).

3.2. Parametric study

This section investigates the effect of various parameters such as the weight fraction, gradient pattern, and dimensions of GPLs, along with the plate's BC and thickness-to-length ratio, on the nonlinear vibration responses of the previously described FG GPL-reinforced composite plate.

Figures 6a-c depict how the weight fraction of GPLs affects the NTL ratio against the dimensionless maximum amplitude curves of FG GPL-reinforced plates with different BCs. The GPLs' gradient pattern is FG-X, and $h/a = 0.1$.

The results revealed that increasing the maximum vibration amplitude for all three contemplated BCs leads to a hardening effect (i.e., an increase in the NTL ratio). In other words, increasing the maximum vibration amplitude intensifies geometrical nonlinearity, leading to an increase in nonlinear frequency. It can also be observed that growing the GPL weight fraction in a fixed dimensionless maximum amplitude decreases the NTL ratio. This is because increasing the GPLs' weight fraction improves the plate's stiffness, reducing the vibration domain, and thus increasing linear and nonlinear frequencies. Nevertheless, the rate of rise in the nonlinear frequency is less than that of the linear frequency, leading to a decrease in the NTL ratio. The effect of adding GPLs on the NTL ratio is significant for low GPL weight fractions but insignificant for higher GPL weight fraction values. The reason is that adding GPLs to pure epoxy significantly increases the plate stiffness and linear frequency. In contrast, higher weight fractions of GPLs slightly affect the plate stiffness and linear frequency.

Figure 7 exhibits the effect of the plate's edge constraints on the NTL ratio while the GPLs' gradient pattern is FG-X, $W_{\mathrm{GPL}} = 0.2\%$, and $h/a = 0.1$.

The results demonstrated that in a fixed maximum vibration amplitude, the maximum NTL ratio corresponds to the SSSS combination of BC, and the minimum one is for the CCCC. More precisely, as BCs are stiffened (i.e., the edge constraints change from simply supported to clamped), linear and nonlinear frequencies represent an increase. However, the effect of stiffened BCs on the linear frequency is more significant than that of the nonlinear frequency. Subsequently, the increase rate of the linear frequency is higher than that of the nonlinear frequency, causing a decrease in the NTL ratio.

Figures 8a-c illustrate the sensitivity examination of the GPL gradient pattern on the variation of the NTL ratio of FG GPL-reinforced composite plates with $W_{\mathrm{GPL}} = 0.2\%$ and $h/a = 0.1$ for three different BC combinations.

Based on the obtained data, the highest natural frequency and the lowest NTL ratio correspond to the FG-X gradient pattern. A higher concentration of GPLs near the upper and lower surfaces of the plate results in the higher stiffness and lower vibration domain, thus increasing the linear and nonlinear frequencies.

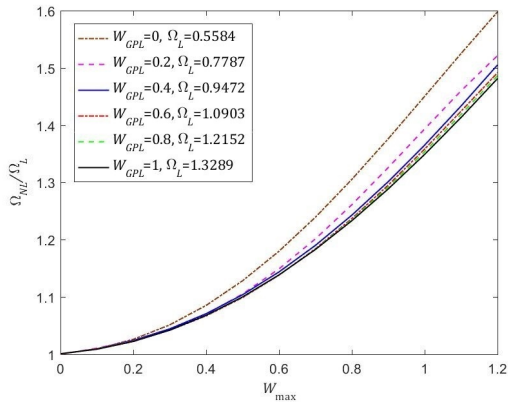

(a) SSSS

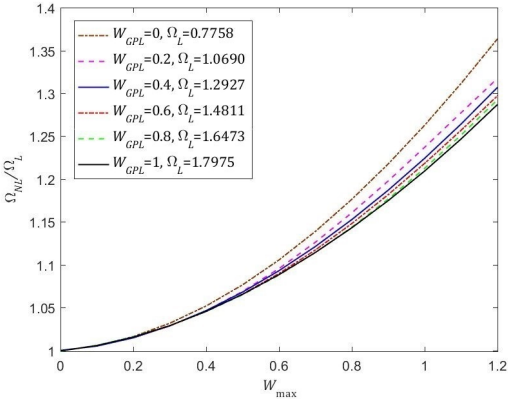

(b) CCSS

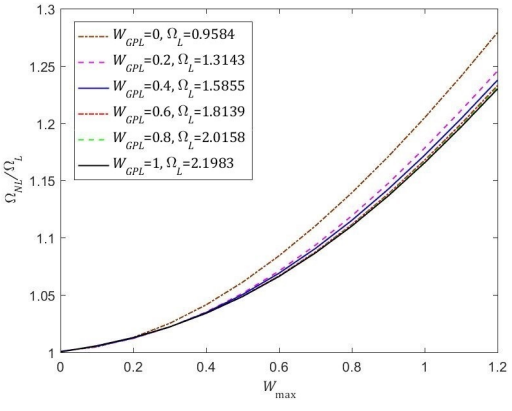

(c) CCCC

Fig. 6. The NTL ratio of GPL/Epoxy FG square plates with different weight fractions of GPL against dimensionless maximum amplitude while the GPL gradient pattern is FG-X ($h/a = 0.1$).

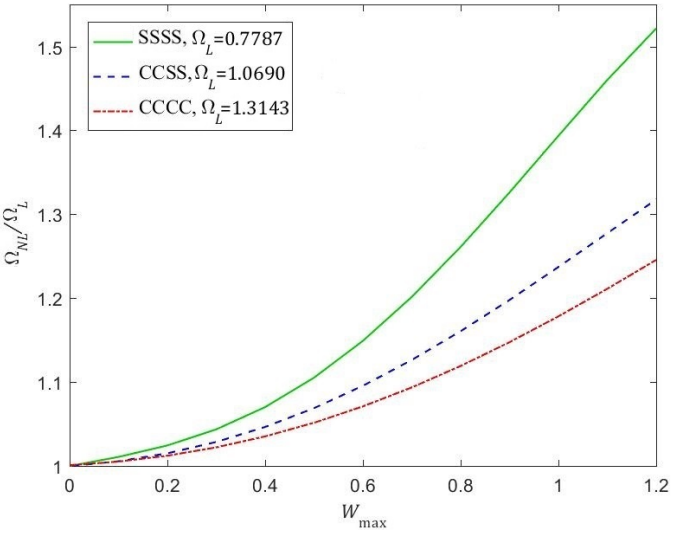

FIG. 7. The NTL ratio of GPL/Epoxy FG square plates with different BCs against dimensionless maximum amplitude while the GPL gradient pattern is FG-X ($W_{\mathrm{GPL}} = 0.2\%$, $h/a = 0.1$).

However, this rise in frequency is smaller for nonlinear than linear frequency, leading to the minimization of the NTL ratio. On the other hand, the highest NTL ratio pertains to the FG-O pattern, whereas the lowest natural frequency is for the plate made of pure epoxy. Furthermore, the results revealed that NTL ratios are equal for the UD pattern and the plate made of pure epoxy because the rate of increase in linear and nonlinear frequencies are exactly equal when the material changes from pure epoxy to the UD pattern.

Figures 9a-c display the effect of the thickness-to-length ratio (h/a) on the NTL ratio, while the GPLs' gradient pattern is FG-O, $W_{\mathrm{GPL}} = 0.2\%$, and BCs are SSSS, CCSS, and CCCC, respectively.

According to the results, with the growing plate thickness, the NTL ratio increases for fixed values of the dimensionless maximum amplitude. The reason is that the nonlinearity is intensified with increasing thickness, and consequently, the rate of increase in the nonlinear frequency exceeds that of the linear frequency.

In the previous figures and table, the GPLs' dimensions were presumed to be constant. Figures 10a-c depict the influence of change in GPLs' average thickness-to-length ratio ($h_{\mathrm{GPL}}/a_{\mathrm{GPL}}$) on the NTL ratio of FG GPL-reinforced composite plates with three various combinations of BCs, while the gradient pattern of GPLs is FG-X, the average thickness of GPLs is constant, $W_{\mathrm{GPL}} = 0.3\%$, and $h/a = 0.1$.

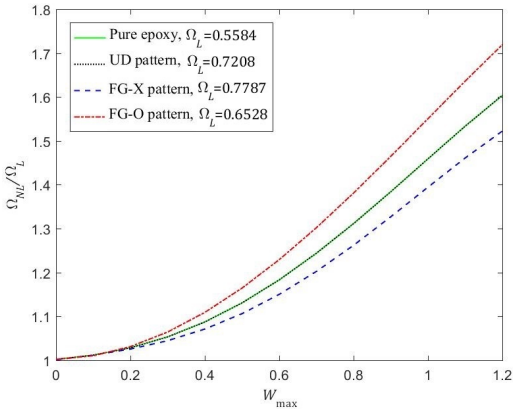

(a) SSSS

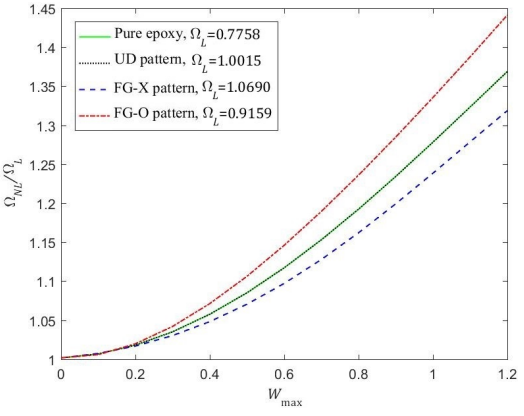

(b) CCSS

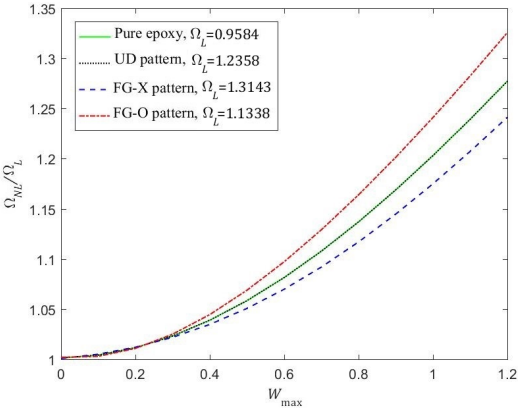

(c) CCCC

Fig. 8. The NTL ratio of GPL/Epoxy FG square plates with different GPL gradient patterns against dimensionless maximum amplitude ($W_{\mathrm{GPL}} = 0.2\%$, $h/a = 0.1$).

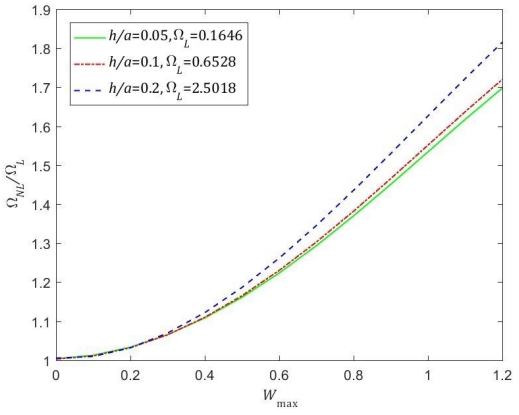

(a) SSSS

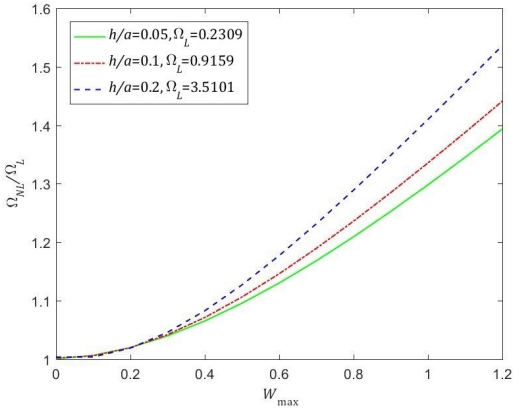

(b) CCSS

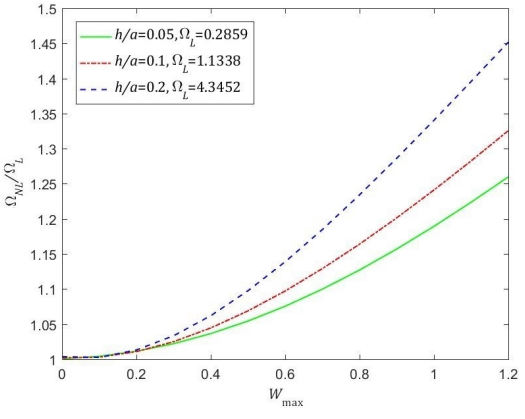

(c) CCCC

FIG. 9. The NTL ratio of GPL/Epoxy FG square plates with FG-O gradient pattern for different thickness-to-length ratios against dimensionless maximum amplitude ($W_{\mathrm{GPL}} = 0.2\%$).

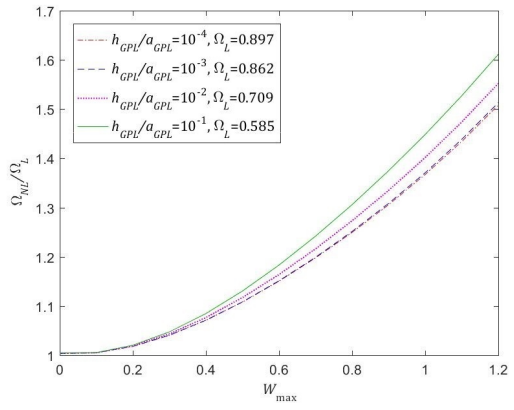

(a) SSSS

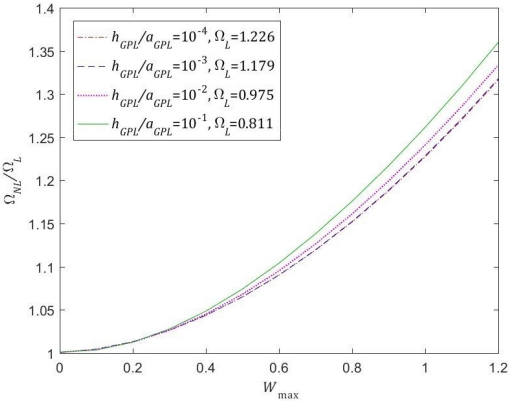

(b) CCSS

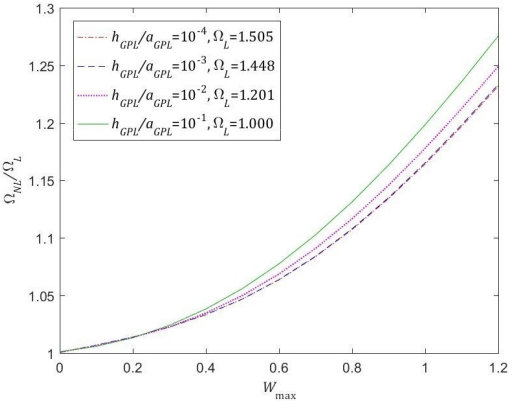

(c) CCCC

Fig. 10. The NTL ratio of GPL/Epoxy FG square plates with various GPL's thickness-to-length ratios against dimensionless maximum amplitude ($W_{\mathrm{GPL}} = 0.3\%$, $h/a = 0.1$).

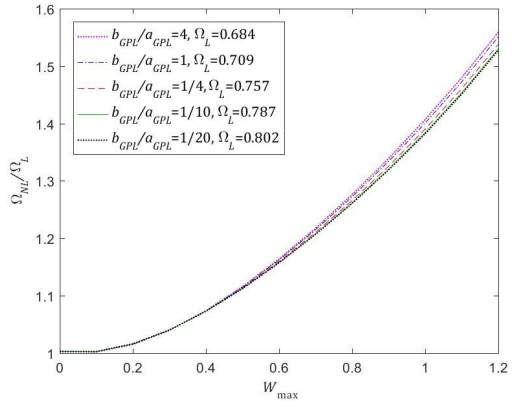

(a) SSSS

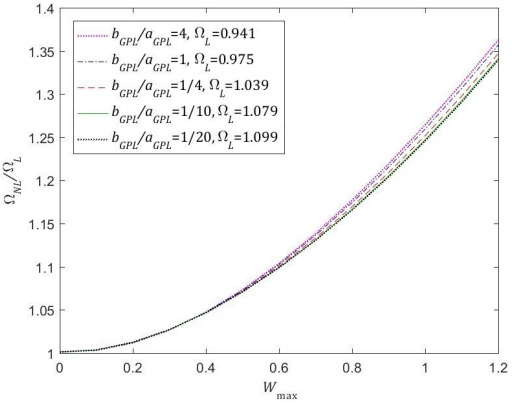

(b) CCSS

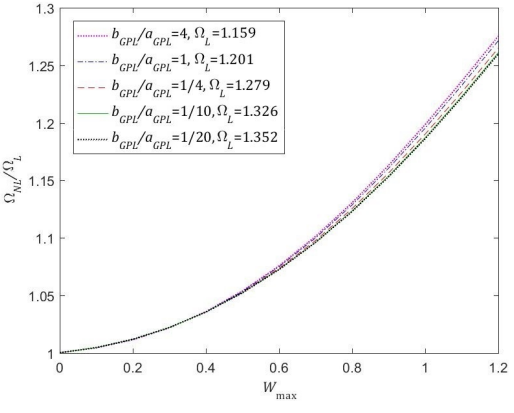

(c) CCCC

FIG. 11. The NTL ratio of GPL/Epoxy FG square plates with different GPL's width-to-length ratios against dimensionless maximum amplitude ($W_{\mathrm{GPL}} = 0.3\%$).

The results represented that growing the thickness-to-length ratio of GPLs leads to a decline in the natural frequency while an increase in the NTL ratio. This is because by raising the thickness-to-length ratio of GPLs, the load transformation among the matrix and GPLs is weakened, leading to a decrease in the plate stiffness and a subsequent reduction in linear frequency while a rise in the NTL ratio.

Figures 11a-c display the influence of change in GPLs' average width-to-length ratio ($b_{\mathrm{GPL}}/a_{\mathrm{GPL}}$) on the NTL ratio of FG GPL-reinforced composite plates with three different combinations of BCs, while the gradient pattern of GPLs is FG-X, the average width of GPLs is constant, $W_{\mathrm{GPL}} = 0.3\%$, $h/a = 0.1$, and $h_{\mathrm{GPL}}/b_{\mathrm{GPL}} = 0.01$.

The results represented that the variation in the average width-to-length ratio of GPLs has an insignificant effect on the NTL ratio. However, due to the constant width of GPLs, the surface contact area between GPLs and polymer matrix is decreased by increasing the width-to-length ratio of GPLs, leading to weaker load transfer and thus lower structural stiffness and linear and nonlinear frequencies.

4. Conclusions

The current research explored the nonlinear free vibration conducts of thin, moderately thick, and thick FG GPL-reinforced composite rectangular plates with different BC combinations. For the initial time, the nonlinear dynamic equations of the rectangular plate were established based on Hamilton's principle by employing von Karman type of kinematic relations in conjunction with the full LW theory, which considers all 3D effects. The resultant nonlinear eigenvalue problem was resolved using a standard iterative process. Finally, after validating the numerical results and solution procedure, detailed parametric studies were conducted to discuss the influence of the weight fraction, gradient pattern, and dimensions of GPLs, as well as the thickness-to-length ratio of the plate, on the NTL ratio of the FG GPL-reinforced composite plate with different BC combinations.

The following key points can be extracted from the nonlinear free vibration analysis:

- The full LW FEM is as precise as the 3D FEM, providing several advantages, such as a reduction in the computational cost, simplicity of change in mesh, and faster achievement of the element stiffness matrix due to maintaining the 2D structure.
- The veracity of the LW theory is confirmed such that the maximum relative difference between the current numerical results and those in the published papers is less than 6.9%.

- Although the linear and nonlinear frequencies increase as further GPLs are added into the polymer matrix, the effect of adding GPLs on the NTL ratio is more prominent for small weight fractions of GPLs.
- The comparison between the nanocomposite plates with three BC combinations proves that the NTL ratio of the plate with the SSSS edges is maximum, and NTL ratios for the plates with CCSS and CCCC edges are in the consequent orders.
- The comparison between the three gradient patterns demonstrates that the NTL ratio of the plate with the FG-O pattern is maximum, and NTL ratios for UD and FG-X patterns are in the subsequent orders.
- The NTL ratio of the nanocomposite plate increases with an increase in the thickness-to-length ratio of the plate.
- The NTL ratio of the nanocomposite plate demonstrates an increase with the rising thickness-to-length ratio of GPLs. Nevertheless, this rise in the NTL ratio is more significant for the larger thickness-to-length ratios of GPLs.
- Although the effect of the width-to-length ratio of GPLs on the NTL ratio is negligible, the NTL ratio is higher for larger width-to-length ratios of GPLs.

References

1. M.A. Rafiee, J. Rafiee, Z. Wang, H. Song, Z.-Z. Yu, N. Koratkar, *Enhanced mechanical properties of nanocomposites at low graphene content*, ACS Nano, **3**, 12, 3884–3890, 2009. doi: 10.1021/nn9010472.

2. M. Fang, K. Wang, H. Lu, Y. Yang, S. Nutt, *Covalent polymer functionalization of graphene nanosheets and mechanical properties of composites*, Journal of Materials Chemistry, **19**, 7098–7105, 2009, doi: 10.1039/b908220d.

3. J. Liu, H. Yan, K. Jiang, *Mechanical properties of graphene platelet-reinforced alumina ceramic composites*, Ceramics International, **39**, 6215–6221, 2013, doi: 10.1016/j.ceramint.2013.01.041.

4. J.A. King, D.R. Klimek, I. Miskioglu, G.M. Odegard, *Mechanical properties of graphene nanoplatelet/epoxy composites*, Journal of Applied Polymer Science, **128**, 4217–4223, 2013, doi: 10.1002/app.38645.

5. F. Wang, L.T. Drzal, Y. Qin, Z. Huang, *Mechanical properties and thermal conductivity of graphene nanoplatelet/epoxy composites*, Journal of Material Sciences, **50**, 1082–1093, 2015, doi: 10.1007/s10853-014-8665-6.

6. H.-S. Shen, *Nonlinear bending of functionally graded carbon nanotube-reinforced composite plates in thermal environments*, Composite Structures, **91**, 9–19, 2009, doi: 10.1016/j.compstruct.2009.04.026.

7. P. Kumar, J. Srinivas, *Vibration, buckling and bending behavior of functionally graded multi-walled carbon nanotube reinforced polymer composite plates using the layer-*

wise formulation, Composite Structures, **177**, 158–170, 2017, doi: 10.1016/j.compstruct.2017.06.055.

8. S. Jedari Salami, *Free vibration analysis of sandwich beams with carbon nanotube reinforced face sheets based on extended high-order sandwich panel theory*, Journal of Sandwich Structures & Materials, **20**, 2, 219–248, 2018, doi: 10.1177/1099636216649788.
9. R. Gholami, R. Ansari, *Geometrically nonlinear resonance of higher-order shear deformable functionally graded carbon-nanotube-reinforced composite annular sector plates excited by harmonic transverse loading*, The European Physical Journal Plus, **133**, 2, 2018, doi: 10.1140/epjp/i2018-11874-6.
10. M. Rout, A. Karmakar, *Free vibration of rotating pretwisted CNTs-reinforced shallow shells in thermal environment*, Mechanics of Advanced Materials and Structures, **26**, 1808–1820, 2019, doi: 10.1080/15376494.2018.1452317.
11. M. di Sciuva, M. Sorrenti, *Bending, free vibration and buckling of functionally graded carbon nanotube-reinforced sandwich plates, using the extended Refined Zigzag Theory*, Composite Structures, **227**, 111324, 2019, doi: 10.1016/j.compstruct.2019.111324.
12. M. Hosseini, M. Sadeghi-Goughari, S.A. Atashipour, M. Eftekhari, *Vibration analysis of single-walled carbon nanotubes conveying nanoflow embedded in a viscoelastic medium using modified nonlocal beam model*, Archives of Mechanics, **66**, 4, 217–244, 2014.
13. M. Terrones, H. Terrones, *The carbon nanocosmos: novel materials for the twenty-first century*, Philosophical Transactions of the Royal Society of London. Series A: Mathematical, Physical and Engineering Sciences, **361**, 2789–2806, doi: 10.1098/rsta.2003.1262.
14. S.-Y. Fu, X.-Q. Feng, B. Lauke, Y.-W. Mai, *Effects of particle size, particle/matrix interface adhesion and particle loading on mechanical properties of particulate–polymer composites*, Composites Part B: Engineering, **39**, 6, 933–961, 2008, doi: 10.1016/j.compositesb.2008.01.002.
15. M. Song, S. Kitipornchai, J. Yang, *Free and forced vibrations of functionally graded polymer composite plates reinforced with graphene nanoplatelets*, Composite Structures, **159**, 579–588, 2017, doi: 10.1016/j.compstruct.2016.09.070.
16. R. Muni Rami Reddy, W. Karunasena, W. Lokuge, *Free vibration of functionally graded-GPL reinforced composite plates with different boundary conditions*, Aerospace Science and Technology, **78,** 147–156, 2018, doi: 10.1016/j.ast.2018.04.019.
17. C.H. Thai, A.J.M. Ferreira, T.D. Tran, P. Phung-Van, *Free vibration, buckling and bending analyses of multilayer functionally graded graphene nanoplatelets reinforced composite plates using the NURBS formulation*, Composite Structures, **220**, 749–759, 2019, doi: 10.1016/j.compstruct.2019.03.100.
18. C. Feng, S. Kitipornchai, J. Yang, *Nonlinear free vibration of functionally graded polymer composite beams reinforced with graphene nanoplatelets (GPLs)*, Engineering Structures, **140**, 110–119, 2017, doi: 10.1016/j.engstruct.2017.02.052.
19. R. Gholami, R. Ansari, *Nonlinear harmonically excited vibration of third-order shear deformable functionally graded graphene platelet-reinforced composite rectangular plates*, Engineering Structures, **156**, 197–209, 2018, doi: 10.1016/j.engstruct.2017.11.019.
20. R. Gholami, R. Ansari, *Nonlinear stability and vibration of pre/post-buckled multilayer FG-GPLRPC rectangular plates*, Applied Mathematical Modelling, **65**, 627–660, 2019, doi: 10.1016/j.apm.2018.08.038.

21. R. GHOLAMI, R. ANSARI, *On the nonlinear vibrations of polymer nanocomposite rectangular plates reinforced by graphene nanoplatelets: A unified higher-order shear deformable model*, Iranian Journal of Science and Technology, Transactions of Mechanical Engineering, **43**, 603–620, 2019, doi: 10.1007/s40997-018-0182-9.

22. M.Y. ABDOLLAHZADEH JAMALABADI, P. BORJI, M. HABIBI, R. PELALAK, *Nonlinear vibration analysis of functionally graded GPL-RC conical panels resting on elastic medium*, Thin-Walled Structures, **160,** 107370, 2021, doi: 10.1016/j.tws.2020.107370.

23. T. FARSADI, D. ASADI, H. KURTARAN, *Frequency study of functionally graded multilayer graphene platelet-reinforced polymer cylindrical panels*, Archives of Mechanics, **73**, 5-6, 471–498, 2021, doi: 10.24423/aom.3761.

24. M.W. TENG, Y.Q. WANG, *Nonlinear forced vibration of simply supported functionally graded porous nanocomposite thin plates reinforced with graphene platelets*, Thin-Walled Structures, **164**, 107799, 2021, doi: 10.1016/j.tws.2021.107799.

25. J.N. REDDY, *A generalization of two-dimensional theories of laminated composite plates*, Communications in Applied Numerical Methods, **3**, 173–180, 1987, doi: 10.1002/cnm.1630030303.

26. A. NOSIER, R.K. KAPANIA, J.N. REDDY, *Free vibration analysis of laminated plates using a layerwise theory*, American Institute of Aeronautics and Astronautics Journal (AIAA Journal), **31**, 12, 2335–2346, 1993, doi: 10.2514/3.11933.

27. M. SHAKERI, R. MIRZAEIFAR, *Static and dynamic analysis of thick functionally graded plates with piezoelectric layers using layerwise finite element model*, Mechanics of Advanced Materials and Structures, **16**, 561–575, 2019, doi: 10.1080/15376490802625514.

28. S. NIKBAKHT, S. JEDARI SALAMI, M. SHAKERI, *Three dimensional analysis of functionally graded plates up to yielding, using full layer-wise finite element method*, Composite Structures, **182**, 99–115, 2017, doi: 10.1016/j.compstruct.2017.09.022.

29. M. MARJANOVIĆ, N. MARKOVIĆ, E. DAMNJANOVIĆ, R. CVETKOVIĆ, *Three-dimensional stress analysis and design of cross-laminated timber panels using full-layerwise-theory-based finite element method*, Thin-Walled Structures, **157**, 107156, 2020, doi: 10.1016/j.tws.2020.107156.

30. M.S. TAYEBI, S. JEDARI SALAMI, M. TAVAKOLIAN, *Free vibration analysis of functionally graded composite rectangular plates reinforced with graphene nanoplatelets (GPLs) using full layerwise finite element method*, Proceedings of the Institution of Mechanical Engineers, Part C: Journal of Mechanical Engineering Science, 2023, 095440622311662, doi: 10.1177/09544062231166245.

31. J. YANG, H. WU, S. KITIPORNCHAI, *Buckling and postbuckling of functionally graded multilayer graphene platelet-reinforced composite beams*, Composite Structures, **161**, 111–118, 2017, doi: 10.1016/j.compstruct.2016.11.048.

32. P.K. MALLICK, *Fiber-Reinforced Composites*, CRC Press, 2007, doi: 10.1201/9781420005981.

33. J.C. HALPIN, J.L. KARDOS, *The Halpin–Tsai equations: A review*, Polymer Engineering and Science, **16**, 5, 344–352, 1976, doi: 10.1002/pen.760160512.

34. R. GUZMÁN DE VILLORIA, A. MIRAVETE, *Mechanical model to evaluate the effect of the dispersion in nanocomposites*, Acta Materialia, **55**, 9, 3025–3031, 2007, doi: 10.1016/j.actamat.2007.01.007.

35. H. Rostami, S. Jedari Salami, *Large amplitude free vibration of sandwich beams with flexible core and FG Graphene Platelet Reinforced Composite (FG-GPLRC) face sheets based on extended higher-order sandwich panel theory*, Thin-Walled Structures, **180**, 109999, 2022, doi: 10.1016/j.tws.2022.109999.

36. H.R. Mojiri, S.J. Salami, *Free vibration and dynamic transient response of functionally graded composite beams reinforced with graphene nanoplatelets (GPLs) resting on elastic foundation in thermal environment*, Mechanics Based Design of Structures and Machines, **50**, 1872–1892, 2022, doi: 10.1080/15397734.2020.1766492.

37. J.N. Reddy, *Mechanics of Laminated Composite Plates and Shells*, CRC Press, 2003, doi: 10.1201/b12409.

38. R.M. Jones, *Mechanics of Composite Materials*, CRC Press, 2018, doi: 10.1201/9781498711067.

39. G. Prathap, T.K. Varadan, *The large amplitude vibration of hinged beams*, Computers and Structures, **9**, 219–222, 1978, doi: 10.1016/0045-7949(78)90141-4.

40. A. Yasmin, I.M. Daniel, *Mechanical and thermal properties of graphite platelet/epoxy composites*, Polymer, **45**, 24, 8211–8219, 2004, doi: 10.1016/j.polymer.2004.09.054.

41. F. Liu, P. Ming, J. Li, *Ab initio calculation of ideal strength and phonon instability of graphene under tension*, Physical Review B, **76**, 064120, 2007, doi: 10.1103/PhysRevB.76.064120.

Received February 4, 2024; revised version May 31, 2024.
Published online July 15, 2024.